Nano Research 2017, 10(11): 3706–3714
DOI 10.1007/s12274-017-1583-6
Research Article
ISSN 1998-0124
CN 11-5974/O4

Optical properties of conductive silver-nanowire films with different nanowire lengths

Xiaoming Yu[1], Xuan Yu[1] (✉), Jianjun Zhang[2], Liqiao Chen[1], Yunqian Long[1], and Dekun Zhang[2]

[1] *Innovation Application Institute, Zhejiang Ocean University, Zhoushan 316004, China*
[2] *College of Electronic Information and Optical Engineering, Nankai University, Tianjin 300071, China*

Received: 14 December 2016
Revised: 6 March 2017
Accepted: 12 March 2017

KEYWORDS
transparent electrode, silver nanowires, transmittance haze factor, forward scattering and backscattering, reflection-haze factor

ABSTRACT

Transparent electrodes made of silver nanowires (Ag NWs) exhibit a higher flexibility than conventional indium tin oxide electrodes. For this reason, Ag NWs may find applications in future flexible electronic and optoelectronic devices. However, different optoelectronic devices have different specific requirements for Ag NWs. For example, the optical transmittance haze is an important but rarely studied aspect of Ag NW films. In this study, the optical transmittance and optical scattering of long (5–50 μm, L-NWs) and short (1–20 μm, S-NWs) Ag NW films were investigated. The L-NWs exhibited better optical transmission than the S-NWs, whereas the S-NWs exhibited better light-scattering properties than the L-NWs. Our results indicate that the L-NWs are suitable for touch-screen displays, whereas the S-NWs are better suited as transparent conductive films for solar cells. We analyzed the scattering ratio of forward-scattered light to backscattered light for both the L-NWs and S-NWs and discovered that the mesh size affected the scattering ratio. For longer wavelengths, a larger mesh yielded a higher backscattering ratio, whereas a smaller mesh yielded a lower backscattering ratio. We formulated an equation for calculating the reflection haze using the total reflection (Ag NWs/glass), R and the reflection of glass, R_0. The reflection haze of the S-NWs and L-NWs exhibited different trends in the visible–near-infrared region. An omnidirectional scattering model for the Ag NWs was used to evaluate the Ag NW scattering properties. The results of this study have great significance for the evaluation of the performance of Ag NWs in optoelectronic devices.

1 Introduction

Transparent conducting electrodes are critical components of solar cells, touch-screen panels, and light-emitting diodes [1–5]. Indium tin oxide (ITO) thin films have excellent electronic properties but a limited scattering capability; moreover, the scarcity and high production cost of indium limit the industrial

Address correspondence to yuxuan@zjou.edu.cn

applications [6, 7]. Thus, several indium-free transparent electrode materials have been investigated, including silver nanowire (Ag NW) meshes [8–12], carbon nanotubes [13–15], graphene [16–18], and conducting polymers [19, 20]. Among these materials, Ag NW films have attracted substantial interest because of their low sheet resistance and high transmittance. However, the optical properties of Ag NWs of different sizes and Ag NWs prepared via different processes are not fully understood. It is highly desirable to tailor the optical properties of Ag NWs for specific applications.

One of the disadvantages of Ag NW films is the high transmittance haze due to the scattered light in touch-panel display applications [9, 21, 22]. On the other hand, the high transmittance haze is advantageous for applications in solar cells [23, 24]. That is, different optical-haze factors are required for different applications.

The optical scattering properties of Ag NW films are highly dependent on the nanowire length, diameter, and density [8, 25–27]. Longer Ag NWs yield a lower density of nanowires because of the higher conductivity. Smaller-diameter Ag NWs yield less haze in the visible wavelength range because of the reduced light scattering [28, 29]. The transmittance of Ag NWs is also affected by the nanowire quantity, length, and diameter. Ag NWs produce scattered light with various scattering angles. To our knowledge, neither the scattering angle nor the scattering ratio of Ag NWs has been investigated previously. Furthermore, scattering in the direction of the reflection is very useful for display applications, although this has rarely been studied.

In this study, we fabricated Ag NW films with different lengths using the drop-coating method. The optical and structural properties of long-nanowire (L-NW) and short-nanowire (S-NW) films were investigated. The L-NWs exhibited a higher transmittance and lower light scattering than the S-NWs, indicating their applicability for touch-screen displays. S-NWs films, owing to their lower transmittance and higher haze factor than L-NWs, are better suited for thin-film solar cells. To analyze the scattering ratio for the incident and reflected light, we formulated a forward scattered-to-backscattered light equation for the L-NW and S-NW films. We found that the scattering ratio could be tailored by changing the mesh size of the nanowires.

2 Experimental

Ag NWs were synthesized by reducing silver nitrate with ethylene glycol (EG) in the presence of $FeCl_3 \cdot 9H_2O$ and polyvinylpyrrolidone (PVP) [30, 31]. First, 30 mL of EG solutions and 0.23 g of PVP (average molecular weight: 360,000) were stirred vigorously in a 100-mL round flask. After PVP had dissolved, 0.25 g of $AgNO_3$ and 3.2 g of $FeCl_3$ solution (600 μmol/L in EG) were added. The reaction was conducted at 150 ℃ for 1.5 h (S-NWs) and 130 ℃ for 4 h (L-NWs). The reaction product was washed with ethanol three times. The prepared Ag NWs were dispersed in ethanol (0.25 g of $AgNO_3$ precursor dispersed in 75 mL of ethanol) and drop-coated on glass substrates. The suspension was streamed along the longitudinal and transverse directions on the substrate surface. This was followed by air drying and heating at 200 ℃ for 20 min. The resistance of the samples was measured as ~ 20 Ω using a digital multimeter.

The morphology of the films was characterized using scanning electron microscopy (SEM, SUPRA 550 VP). X-ray diffraction (XRD) patterns were obtained using an X-ray diffractometer (D/max-2700). Transmittance spectroscopy was performed on the layers using a spectrophotometer (Cary 5000 UV-Vis-NIR).

The transmittance haze is defined as

$$\text{Haze}_{\text{T}}\,(H_{\text{T}}) = \frac{T_{\text{diffuse}}(\lambda)}{T_{\text{total}}(\lambda)} = \frac{T_{\text{total}} - T_{\text{specular}}}{T_{\text{total}}(\lambda)} \times 100\% \quad (1)$$

The total transmittance (T_{total}) indicates the ability of light to pass through the thin film and was measured using an integrating sphere. The specular transmittance (T_{specular}) was directly measured using a detector with incident light; the light passing directly through the sample was collected. The diffuse transmittance (T_{diffuse}) is defined by the difference between the total transmittance and the specular transmittance. The optical-haze factor is critical for the efficiency of solar cells [32–36]. The haze value is an index that characterizes the scattered light. A longer path of light through the absorbing layer of a solar cell yields a higher current in the solar cell [4, 24].

3 Results and discussion

Figure 1 shows an SEM image of Ag NW films with different lengths and concentrations. The S-NWs were highly concentrated and compacted. The length of the S-NWs ranged from 1 to 20 μm, and the S-NWs had an average length of 8.3 μm and an average diameter of 85 nm (Figs. S1(a) and S1(b) in the Electronic Supplementary Material (ESM)). More than half (67%) of the nanowires were 1–10 μm in length. The L-NWs were sparse compared with the S-NWs and 5–50 μm in length. The L-NWs had an average length of 14.1 μm and an average diameter of 93 nm (Figs. S1(c) and S1(d) in the ESM). The majority of the L-NWs (72%) were 10–20 μm in length. The average length of the L-NWs was nearly twice that of the S-NWs, whereas the average diameter was very similar.

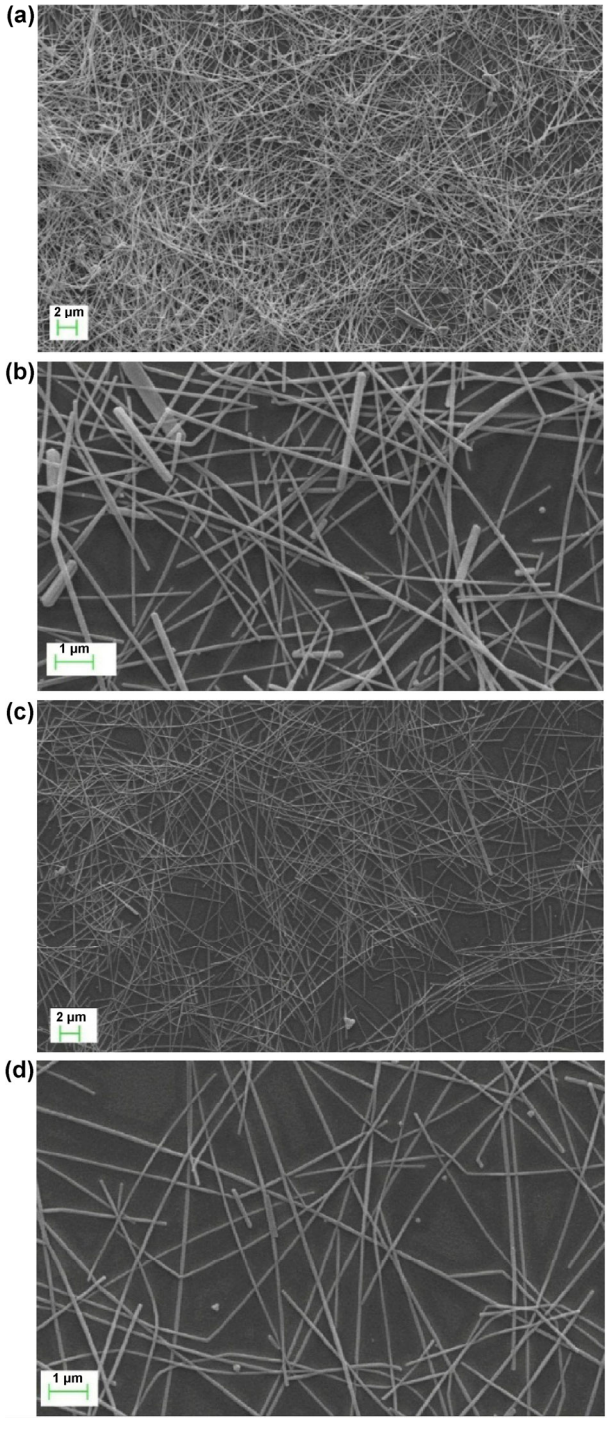

Figure 1 SEM images of the S-Ag NW film ((a) 5k× and (b) 20k×) and the L-Ag NW film ((c) 5k× and (d) 20k×) on glass. The scale bars in the insets correspond to 1,000 nm (b) and (d) and 2,000 nm (a) and (c).

The approximate sheet resistivity was determined. The S-NW density was far higher than L-NW density. The SEM images clearly indicate that there was uniformity in the diameter. Therefore, the major difference in L-NW and S-NWs arose from the nanowire length and density.

The XRD patterns for the S-NWs and L-NWs are shown in Fig. 2. These patterns are indexed as face-centered cubic silver crystals (JCPDS 04-0783), and a strong (111) diffraction peak is observed at 38°. Moreover, there is a (200) orientation peak at 44°. No peak corresponding to silver oxide is observed. The XRD patterns indicate that the S-NWs and L-NWs had the same composition. Figure 3 shows the specular transmittance (ST) and total transmittance (TT) of the S-NW film (a) and the L-NW film (b). The total transmittances of the S-NW and L-NW films in the wavelength range of 400–1,300 nm were

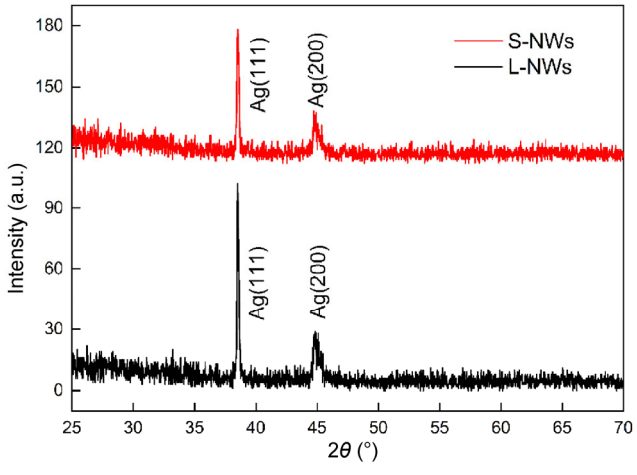

Figure 2 XRD pattern for the S-Ag NW film and the L-Ag NW film on glass.

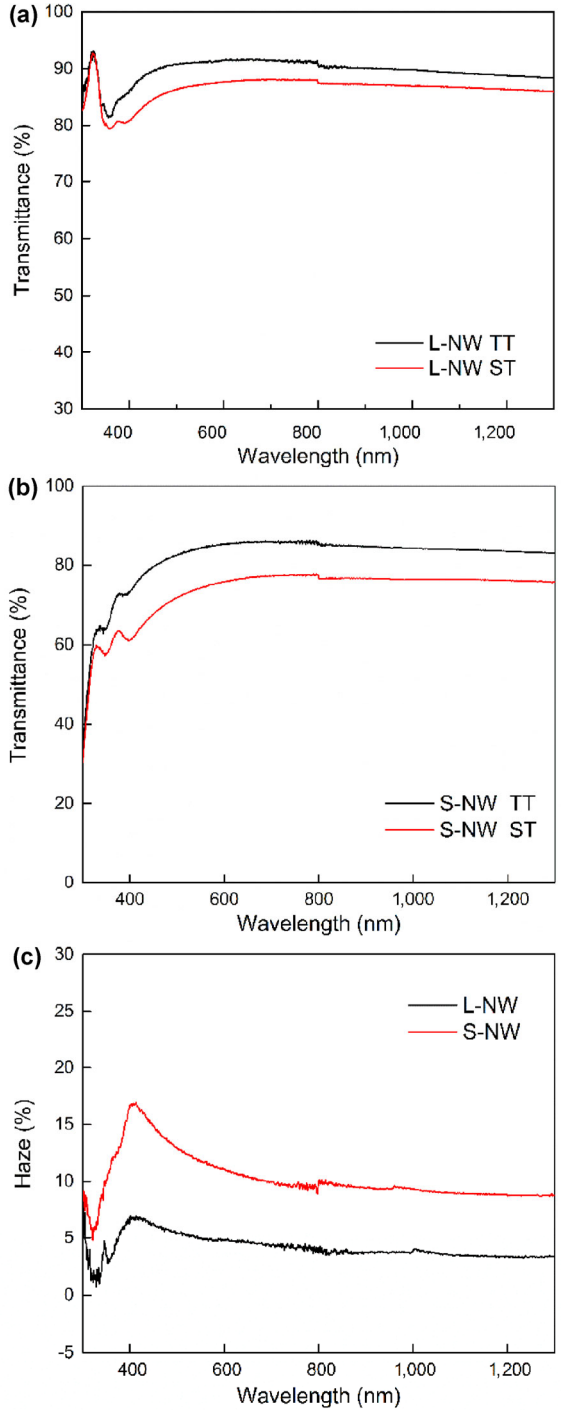

Figure 3 Specular transmittance and total transmittance of the S-Ag NW film (a) and the L-Ag NW film (b). Haze factors of the S-Ag NW and L-Ag NW films (c) (glass deducted).

approximately 82%–87% (average of 85.31%) and 86%–91% (average of 89.67%), respectively. The S-NW film had a slightly lower total transmittance (by ~ 4%) than the L-NW film. The total transmittance did not exhibit a large variation with respect to the length and density of the nanowires. All the spectra exhibited a wide flat region from 450 to 1,300 nm, with the exception of strong reductions of the transmittance in the range of 300–400 nm for the S-NWs, which were due to the large amount of surface plasmons generated by the short nanorods [37]. The reductions of the transmittance for the L-NWs were approximately 350 nm and were due to the surface plasmons generated by the longer nanowires.

On the other hand, the specular transmittance decreased as the amount of nanowires increased. The specular transmittances of the S-NW and L-NW films in the wavelength range of 400–1,300 nm were approximately 74%–78% (average of 77.74%) and 80%–88% (average of 86.56%), respectively. Examining the trend of the ST using the SEM micrographs of Fig. 1 reveals that a larger amount of nanowires yielded a lower ST, which increased the light scattered by the Ag NW film.

The H_T of the S-NW and L-NW films is shown in Fig. 3(c). The H_T of the S-NWs decreased from 17% to 9% as the wavelength increased from 400–1,300 nm. The H_T of the L-NWs decreased from 7% to 3% for the same wavelength change. The haze factor for the S-NW film was twice as large as that for the L-NW film. The H_T clearly indicated significant light scattering for the S-NW film over the full spectral range compared with the L-NWs. The SEM images in Fig. 1 show that the number of S-NWs was about twice as large as the number of L-NWs. The average haze in the wavelength range of 400–1,300 nm for the S-NWs and L-NWs was 10.28 and 4.16, respectively. The H_T of the Ag NW film depended on several factors: the length and diameter of the nanowires, the nanowire density, and fabrication method [25–27]. As reported by T. Araki et al. [25], there was a small difference in the optical haze between different diameter nanowires. The haze for nanowires 91 nm in diameter was 1%–1.5% higher than that of nanowires 68 nm in diameter and with approximately the same length. The S-NWs had an average diameter of 85 nm, and the L-NWs had an average diameter of 93 nm. The average diameter and statistical distribution were similar between the L-NWs and S-NWs. Rather than the diameter, the length was the major difference between the L-NWs and S-NWs. Therefore, we consider that the diameter

had a small effect on the scattering. The differences in the optical properties arose from the differences in the length and density.

The haze factor for the Ag NW network was determined using the NW density and other properties. Larger haze values for S-NWs correspond to increased scattering due to a higher nanowire density.

The transmittance of the Ag NW films for both the S-NWs and L-NWs in the wavelength range of 400–1,300 nm range was higher than 80%, which indicates a high transparency. As in our previous study [24], the Ag NW films exhibited extremely low absorption in the range of 400–1,300 nm. In addition to a lower amount of light being absorbed by the Ag NW film, the majority of the non-transmitted light was scattered by the Ag NWs. Effectively managing the light backscattered by Ag NW thin films is a topic for future research.

Ag NWs scatter light in all directions. The scattered light can be divided into two parts: the forward-scattered light (0°–180°) and backscattered light (180°–360°). To our knowledge, there is no clear definition for forward-scattered or backscattered light. The ratio of forward-scattered light to backscattered light is not discussed in the literature.

Herein, we define $R_{\text{diffuse}} = R - R_0$ as the backscattered light. R represents the total optical reflection of the Ag NW film on glass measured using an integrating sphere, and R_0 is the reflection of the glass. The degree of forward-scattered light is defined as T_{diffuse} = TT – ST, where TT is the total transmittance measured an integrating sphere, and ST is the specular transmittance. A schematic of the transmittance, reflection of glass, and Ag NWs is shown in Fig. S2 in the ESM.

$$R_{\text{diffuse}} = R - R_0 \tag{2}$$

$$T_{\text{diffuse}} = \text{TT} - \text{ST} \tag{3}$$

Total-scattered light

$$T_{\text{s}} = R_{\text{diffuse}} + T_{\text{diffuse}} = (R - R_0) + (\text{TT} - \text{ST}) \tag{4}$$

$$R_{\text{Fs}} = T_{\text{diffuse}} / T_{\text{s}} \tag{5}$$

$$R_{\text{Bs}} = R_{\text{diffuse}} / T_{\text{s}} \tag{6}$$

The forward-scattered and backscattered light can be easily calculated using the total transmittance, specular transmittance, total reflectance, and reflectance of glass. Figure 4(a) shows the forward-scattered and backscattered light for the L-NWs with respect to the wavelength in the range of 400–1,400 nm. As the wavelength increased, the forward-scattered light decreased, whereas the backscattered light initially decreased and then increased. The total scattered light exhibited a similar trend to the backscattered light. For the L-NW film, the backscattering capability was stronger than the forward-scattering capability. We calculated the scattering ratio using Eqs. (3) and (4). As shown in Fig. 4(b), as the wavelength increased from 400 to 1,500 nm, the backscattering ratio for the L-NWs increased from 53% to 73%, whereas the forward-scattering ratio for L-NWs decreased from 47% to 27%. As the wavelength increased from 400 to 1,500 nm, the scattering ratio for the L-NWs gradually

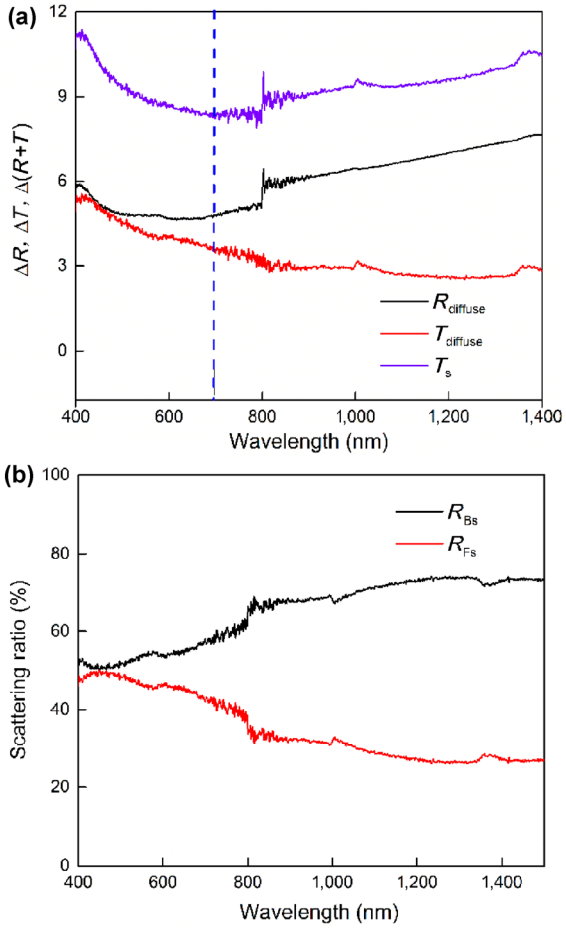

Figure 4 R_{diffuse}, T_{diffuse}, and T_{s} for the L-Ag NW film (a) and ratio of backscattered light to forward-scattered light for the L-Ag NW film (b).

changed: The backscattering increased, and the forward scattering decreased.

The forward-scattered and backscattered light exhibited a different trend for the S-NWs than for the L-NWs. Figure 5(a) shows the forward-scattered, backscattered, and total scattered light for the S-NWs with respect to the wavelength for the wavelength range of 400–1,300 nm. The scattered light initially increased at wavelengths of 300–500 nm and then decreased with increased further. The forward-scattered and backscattered light exhibited similar trends and values.

We calculated the scattering ratio using Eqs. (3) and (4), as shown in Fig. 5. As the wavelength increased from 400–1,300 nm, the forward-scattering ratio for the S-NWs decreased from 55% to 47%, and the backscattering ratio for the S-NWs increased from 45% to 53%. Both the forward-scattering and backscattering ratios remained relatively constant throughout the spectrum.

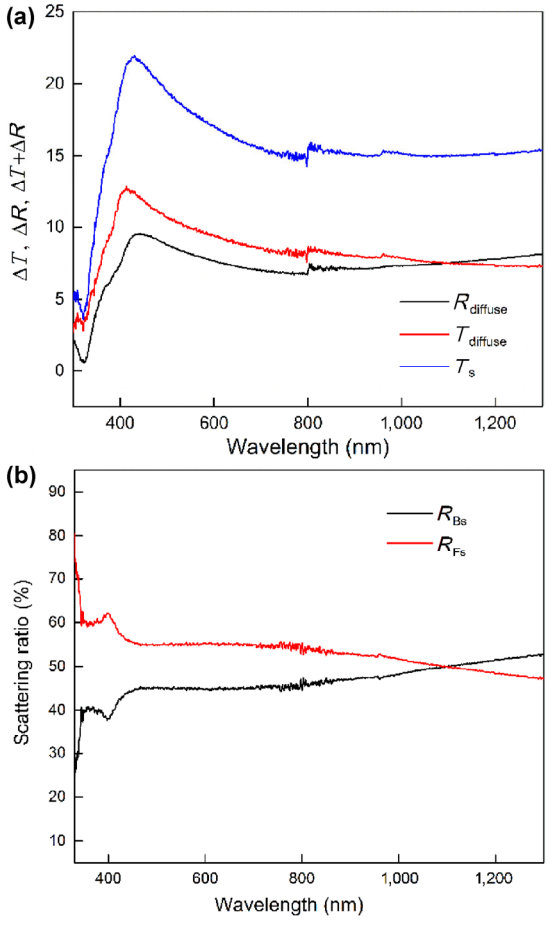

Figure 5 $R_{diffuse}$, $T_{diffuse}$, and T_s for the S-Ag NW film (a) and the ratio of backscattered light to forward-scattered light for the S-Ag NW film (b).

The scattering ratio at a specific wavelength can be tuned by changing the length and density of the nanowires. According to the SEM images and Fig. 4, the L-NW thin film had a larger mesh because of the lower density of nanowires. Longer-wavelength light yielded a larger forward-scattering ratio for the L-NWs and a slightly smaller forward-scattering ratio for the S-NWs. Thus, the mesh size of the nanowires affected the scattering ratio. A larger mesh yielded more backscattering at longer wavelengths, and smaller mesh yielded a smaller backscattering ratio at longer wavelengths. The light backscattered by the NW thin film was scattered not only by individual the nanowires but also by the nanowires forming meshes. This observation opposes the generally accepted idea that increasing or decreasing the nanowire density changes the forward-scattering and backscattering ratios.

To elucidate the proportion of diffuse reflection in the total reflection, the reflection haze of the Ag NWs was defined as

$$H_R = \frac{R_{diffuse}(\lambda)}{R_{total}(\lambda)} = \frac{R - R_0}{R} \times 100\% \quad (7)$$

The H_R values for the S-NW and L-NW films are shown in Fig. 6. Although $R_{diffuse}$ is smaller than $T_{diffuse}$, the reflection R is four times smaller than the total

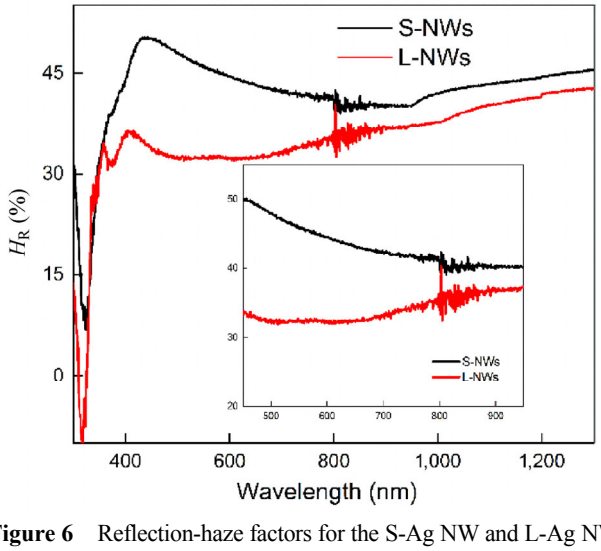

Figure 6 Reflection-haze factors for the S-Ag NW and L-Ag NW films, calculated according to the total reflection.

transmittance, indicating that H_R is three times larger than the haze calculated using the transmittance. The H_R for the S-NWs initially increased to 45% at 440 nm, decreased to 40% at 940 nm, and then increased to 45% at 1,300 nm. The H_R for the L-NW film was smaller than that for the S-NW films in the measured region. The H_R for the L-NWs initially increased to 36% at 400 nm, decreased to 32% around 500–650 nm, and then increased to 42% at 1,300 nm. As shown in Fig. 6, the H_R values for the S-NWs and L-NWs exhibited different trends in the wavelength range of 500–1,000 nm. Preston et al. theoretically investigated the H_T factor for Ag NWs using finite-difference time-domain simulations [29]. The simulations indicated that the scattering fields produced by Ag NWs are not restricted to small angles. Rather, they extend to larger forward-scattering angles as well. Hence, the scattering fields have a space distribution of 0°–360°. The Ag NW film forms a two-dimensional (2D) mesh grid with a random distribution of NWs on the glass substrate. When light travels through a disordered system, scattering-enhancement phenomena are commonly caused by the coherent-backscattering effect. A phase difference of zero between the backscattered light and the light reflected by the glass surface may result in the coherent-backscattering effect. The impact of diffuse scattered light must be addressed. A large amount of backscattered light, which causes a large H_R of Ag NWs, is important for displays. In this paper, we introduced a series of formulas for evaluating the light forward-scattered and backscattered by Ag NWs. The H_R factor can be treated as a new figure of merit.

4 Conclusion

The haze values for S-NW and L-NW films were compared. The S-NW films, which have a larger haze value and more forward-scattered light, can be used in thin-film solar cells. We developed an equation for calculating the ratio of forward-scattered light to backscattered light in order to characterize the forward scattering and backscattering of Ag NW films. Different scattering ratios were obtained for the S-NW and L-NW films. We also defined and calculated the reflection-haze factor for the S-NW and L-NW films. We consider that the light backscattered by the NW thin films was scattered not only by the individual nanowires but also by the meshes formed by the nanowires. We used a series of equations to define the forward-scattering and backscattering properties of Ag NWs. The discovery of Ag NW light scattering in different directions is relevant for many practical applications with transparent conducting electrodes and thus has great practical significance. The unique optical scattering of Ag NWs (separate wires forming a 2D mesh) compared with conventional continuous thin films allows the development of novel optical-evaluation systems. The interaction of light with Ag NWs should be further studied owing to its great significance for the practical application of Ag NWs in transparent conductive films.

Acknowledgements

This work was supported from the National Natural Science Foundation of China (Nos. 11604298 and 61377031) and Scientific Research Foundation (Nos. Q1444 and 1539) of Zhejiang Ocean University.

Electronic Supplementary Material: Supplementary material (length statistical distribution and schematic diagram of transmittance, reflection of Ag nanowires) is available in the online version of this article at https://doi.org/10.1007/s12274-017-1583-6.

References

[1] Bae, S.; Kim, H.; Lee, Y.; Xu, X. F.; Park, J. S.; Zheng, Y.; Balakrishnan, J.; Lei, T.; Kim, H. R.; Song, Y. et al. Roll-to-roll production of 30-inch graphene films for transparent electrodes. *Nat. Nanotechnol.* **2010**, *5*, 574–578.

[2] Li, X. S.; Zhu, Y. W.; Cai, W. W.; Borysiak, M.; Han, B. Y.; Chen, D.; Piner, R. D.; Colombo, L.; Ruoff, R. S. Transfer of large-area graphene films for high-performance transparent conductive electrodes. *Nano Lett.* **2009**, *9*, 4359–4363.

[3] Minami, T. Transparent conducting oxide semiconductors for transparent electrodes. *Semicond. Sci. Technol.* **2005**, *20*, S35–S44.

[4] Hecht, D. S.; Hu, L. B.; Irvin, G. Emerging transparent electrodes based on thin films of carbon nanotubes,

graphene, and metallic nanostructures. *Adv. Mater.* **2011**, *23*, 1482–1513.

[5] Wang, X.; Zhi, L. J.; Müllen, K. Transparent, conductive graphene electrodes for dye-sensitized solar cells. *Nano Lett.* **2008**, *8*, 323–327.

[6] Jansseune, T. Indium price soars as demand for displays continues to grow. *Comp. Semicond.* **2005**, *11*, 34–35.

[7] Boehme, M.; Charton, C. Properties of ITO on PET film in dependence on the coating conditions and thermal processing. *Surf. Coat. Technol.* **2005**, *200*, 932–935.

[8] Lee, J. Y.; Connor, S. T.; Cui, Y.; Peumans, P. Solution-processed metal nanowire mesh transparent electrodes. *Nano Lett.* **2008**, *8*, 689–692.

[9] Hu, L. B.; Kim, H. S.; Lee, J. Y.; Peumans, P.; Cui, Y. Scalable coating and properties of transparent, flexible, silver nanowire electrodes. *ACS Nano* **2010**, *4*, 2955–2963.

[10] De, S.; Higgins, T. M.; Lyons, P. E.; Doherty, E. M.; Nirmalraj, P. N.; Blau, W. J.; Boland, J. J.; Coleman, J. N. Silver nanowire networks as flexible, transparent, conducting films: Extremely high DC to optical conductivity ratios. *ACS Nano* **2009**, *3*, 1767–1774.

[11] Khanarian, G.; Joo, J.; Liu, X. Q.; Eastman, P.; Werner, D.; O'Connell, K.; Trefonas, P. The optical and electrical properties of silver nanowire mesh films. *J. Appl. Phys.* **2013**, *114*, 024302.

[12] Jiu, J. T.; Murai, K.; Kim, D.; Kim, K.; Suganuma, K. Preparation of Ag nanorods with high yield by polyol process. *Mater. Chem. Phys.* **2009**, *114*, 333–338.

[13] Baughman, R. H.; Zakhidov, A. A.; de Heer, W. A. Carbon nanotubes—The route toward applications. *Science* **2002**, *297*, 787–792.

[14] Yakobson, B. I.; Avouris, P. Mechanical properties of carbon nanotubes. In *Carbon Nanotubes*; Dresselhaus, M. S.; Dresselhaus, G.; Avouris, P., Eds.; Springer: Berlin, Heidelberg, 2001; pp 287–327.

[15] Niu, C. M.; Sichel, E. K.; Hoch, R.; Moy, D.; Tennent, H. High power electrochemical capacitors based on carbon nanotube electrodes. *Appl. Phys. Lett.* **1997**, *70*, 1480–1482.

[16] Wu, J. B.; Becerril, H. A.; Bao, Z.; Liu, Z. F.; Chen, Y. S.; Peumans, P. Organic solar cells with solution-processed graphene transparent electrodes. *Appl. Phys. Lett.* **2008**, *92*, 263302.

[17] Kim, K. S.; Zhao, Y.; Jang, H.; Lee, S. Y.; Kim, J. M.; Kim, K. S.; Ahn, J. H.; Kim, P.; Choi, J. Y.; Hong, B. H. Large-scale pattern growth of graphene films for stretchable transparent electrodes. *Nature* **2009**, *457*, 706–710.

[18] Zhang, Q. C.; Tang, L.; Luo, J.; Zhang, J.; Wang, X. N.; Li, D.; Yao, Y. G.; Zhang, Z. X. Direct growth of nanocrystalline graphene/graphite all carbon transparent electrode for graphene glass and photodetectors. *Carbon* **2017**, *111*, 1–7.

[19] Gustafsson, G.; Cao, Y.; Treacy, G. M.; Klavetter, F.; Colaneri, N.; Heeger, A. J. Flexible light-emitting diodes made from soluble conducting polymers. *Nature* **1992**, *357*, 477–479.

[20] Zou, J. Y.; Yip, H. L.; Hau, S. K.; Jen, A. K. Y. Metal grid/conducting polymer hybrid transparent electrode for inverted polymer solar cells. *Appl. Phys. Lett.* **2010**, *96*, 203301.

[21] Kiran Kumar, A. B. V.; Wan Bae, C.; Piao, L. H.; Kim, S. H. Silver nanowire based flexible electrodes with improved properties: High conductivity, transparency, adhesion and low haze. *Mater. Res. Bull.* **2013**, *48*, 2944–2949.

[22] Kim, T.; Canlier, A.; Kim, G. H.; Choi, J.; Park, M.; Han, S. M. Electrostatic spray deposition of highly transparent silver nanowire electrode on flexible substrate. *ACS Appl. Mater. Interfaces* **2013**, *5*, 788−794.

[23] Langley, D. P.; Giusti, G.; Lagrange, M.; Collins, R.; Jiménez, C.; Bréchet, Y.; Belleta, D. Silver nanowire networks: Physical properties and potential integration in solar cells. *Sol. Energ. Mat. Sol. C.* **2014**, *125*, 318–324.

[24] Yu, X. M.; Yu, X.; Zhang, J. J.; Zhang, D. K.; Ni, J.; Cai, H. K.; Zhang D. X.; Zhao, Y. Investigation of light transmission and scattering properties in silver nanowire mesh transparent electrodes. *Mater. Lett.* **2015**, *145*, 219–223.

[25] Araki, T.; Jiu, J. T.; Nogi, M.; Koga, H.; Nagao, S.; Sugahara, T.; Suganuma, K. Low haze transparent electrodes and highly conducting air dried films with ultra-long silver nanowires synthesized by one-step polyol method. *Nano Res.* **2014**, *7*, 236–245.

[26] Liu, Y.; Chen, Y. Y.; Shi, R.; Cao, L. J.; Wang, Z.; Sun, T.; Lin, J. J.; Liu, J. Q.; Huang, W. High-yield and rapid synthesis of ultrathin silver nanowires for low-haze transparent conductors. *RSC Adv.* **2017**, *7*, 4891–4895.

[27] Sorel, S.; Lyons, P. E.; De, S.; Dickerson, J. C.; Coleman, J. N. The dependence of the optoelectrical properties of silver nanowire networks on nanowire length and diameter. *Nanotechnology* **2012**, *23*, 185201.

[28] Katagiri, K.; Hunakubo, T. Metal nanowires, method for producing same, transparent conductor and touch panel. U.S. Patent 20120255762 A1, Oct. 11, 2012.

[29] Colin, P.; Xu, Y. L.; Han, X. G.; Munday, J. N.; Hu, L. B. Optical haze of transparent and conductive silver nanowire films. *Nano Res.* **2013**, *6*, 461–468.

[30] Jiu, J.; Araki, T.; Wang, J.; Nogi, M.; Sugahara, T.; Nagao, S.; Koga, H.; Suganuma, K.; Nakazawa, E.; Hara, M. et al. Facile synthesis of very-long silver nanowires for transparent electrodes. *J. Mater. Chem. A* **2014**, *2*, 6326–6330.

[31] Tokuno, T.; Nogi, M.; Karakawa, M.; Jiu, J. T.; Nge, T. T.; Aso, Y.; Suganuma, K. Fabrication of silver nanowire transparent electrodes at room temperature. *Nano Res.* **2011**, *4*, 1215–1222.

[32] Tsai, C.-H.; Hsu, S.-Y.; Huang, T.-W.; Tsai, Y.-T.; Chen, Y.-F.; Yuan, H. J.; Lun, H.; Wu, C.-C.; Chen, Y.-S.; Chen, C.-W. et al. Influences of textures in fluorine-doped tin oxide on characteristics of dye-sensitized solar cells. *Org. Electron*. **2011**, *12*, 2003–2011.

[33] Chiba, Y.; Islam, A.; Watanabe, Y.; Komiya, R.; Koide, N.; Han, L. Y. Dye-sensitized solar cells with conversion efficiency of 11.1%. *Jpn. J. Appl. Phys*. **2006**, *45*, L638.

[34] Kluth, O.; Rech, B.; Houben, L.; Wieder, S.; Schöpe, G.; Beneking, C.; Wagner, H.; Löffl, A.; Schock, H. W. Texture etched ZnO:Al coated glass substrates for silicon based thin film solar cells. *Thin Solid Films* **1999**, *351*, 247–253.

[35] Fang, Z. Q.; Zhu, H. L.; Yuan, Y. B.; Ha, D.; Zhu, S. Z.; Preston, C.; Chen, Q. X.; Li, Y. Y.; Han, X. G.; Lee, S. et al. Novel nanostructured paper with ultrahigh transparency and ultrahigh haze for solar cells. *Nano Lett*. **2014**, *14*, 765–773.

[36] Zhang, S. T.; Foldyna, M.; Roussel, H.; Consonni, V.; Pernot, E.; Schmidt-Mende, L.; Rapenne, L.; Jiménez, C.; Deschanvres, J.-L.; Muñoz-Rojas, D. et al. Tuning the properties of F:SnO_2 (FTO) nanocomposites with S:TiO_2 nanoparticles-promising hazy transparent electrodes for photovoltaics applications. *J. Mater. Chem. C* **2017**, *5*, 91–102.

[37] Tao, A.; Kim, F.; Hess, C.; Goldberger, J.; He, R. R.; Sun, Y. G.; Xia, Y. N.; Yang, P. D. Langmuir–Blodgett silver nanowire monolayers for molecular sensing using surface-enhanced Raman spectroscopy. *Nano Lett.* **2003**, *3*, 1229–1233.